Carbohydrate Polymers 327 (2024) 121657

Contents lists available atScienceDirect

Carbohydrate Polymers

journal homepage: www.elsevier.com/locate/carbpol

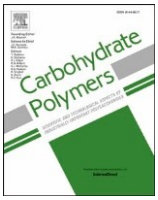

A multifunctional cellulose- and starch-based composite hydrogel with iron-modified biochar particles for enhancing microalgae growth

Bahare Salehi [a], Bo Zhang [b], Kyle Nowlin [a], Lijun Wang [b,c,*], Abolghasem Shahbazi [b,c]

[a] Joint School of Nanoscience and Nanoengineering, North Carolina Agricultural and Technical State University, Greensboro, NC, USA [b] Department of Natural Resources and Environmental Design, North Carolina Agricultural and Technical State University, Greensboro, NC, USA [c] Department of Chemical, Biological, and Bioengineering, North Carolina Agricultural & Technical State University, Greensboro, NC, USA

ARTICLEINFO

Keywords: A multifunctional polysaccharide-based hydrogel was studied as an additive for enhancing microalgae growth. Microalgae The hydrogel was fabricated by physically and chemically crosslinking renewable ingredients of carboxymethyl

Hydrogel Biochar Nanomaterials

ABSTRACT

Attached algae growth cellulose (CMC), arrowroot starch, and activated biochar modified with iron using a bio-crosslinker of oxidized sucrose and a plasticizer of glycerol. The optimum formula for the hydrogel with a high swelling ratio, BET surface area, and electrical conductivity was found to include 1 g starch, 3 g CMC, 1.5 g biochar, 15 mL oxidized sucrose, and 1.5 mL glycerol in 200 mL deionized water. The algal yield and cell concentration after 14 days of growth in a Bold basal medium with an optimum concentration of 2.5 g hydrogel/L increased by 65.7 % and 92.2 %, respectively, compared to those of the control without the hydrogel. However, if the hydrogel concentration in the culture increased to 12.5 g/L, the algal yield was decreased by 67.8 % compared to the control due to oxidative injury. The hydrogel additive could significantly increase the nitrogen but decrease the carbon, hydrogen, and sulfur contents of the microalgae. The algal yield with 2.5 g/L hydrogel additive improved by 13.9 % compared to the algal yield with the same amounts of individual non–crosslinked hydrogel ingredients.

1. Introduction

Microalgae have been used for many environmental applications such as wastewater treatment and CO_2 sequestration, and commercial production of biofuels, biochar, bio-chemicals, bioplastics, feed, and fertilizers (Ansah, Wang, Zhang, & Shahbazi, 2018; Mathiot et al., 2019; Rahman, Zhang, Wang, & Shahbazi, 2019; Zhang, Wang, Li, Rahman, & Shahbazi, 2017). Low biomass density and difficulty in harvesting are major technical and economic obstacles to the commercialization of suspended microalgal cultivation which can be addressed in attached microalgae growth systems by forming a thin layer of microalgal film onto a solid surface (Rosli et al., 2020).

Biochar loaded with iron oxide can be used as a magnetic porous support to enhance algal attachment and growth (Thomas, Fernandez, Mullassery, & Surya, 2020). Furthermore, magnetic nanostructured biochar can adsorb and concentrate nutrients from agricultural wastewater for wastewater treatment to support algal growth (White, Strosnider, Chase, & Schlautman, 2021). The effectiveness of biochar can be significantly improved by being part of the three dimensional (3D) cross- linked network of hydrogel through improved hydrophilicity, favorable modifiability, swellability, and sorption capacity of the biochar- hydrogel composite (Das, Ghosh, & Avasthe, 2021; Karakoyun et al., 2011). Hydrogel is a 3D porous network of hydrophilic polymers that can absorb and retain large quantities of water, which has wide applications in biomedicine, wastewater treatment, hygiene and slow-release fertilizers (Liu, Wang, Chen, & Cheng, 2022; Qureshi, Nishat, Jadoun, & Ansari, 2020).

There is an increasing tendency to use bio-based polymers such as starch and carboxymethyl cellulose (CMC) to make hydrogel due to their abundancy, renewability, nontoxicity, and biodegradability (Chen & Chen, 2019; Cui et al., 2022; Fekete, Borsa, Takacs, ´ & Wojnarovits, ´ 2017; Qureshi et al., 2020). It was found that the starch and CMC composite hydrogel had better gelation and water absorption capacity than those hydrogels with starch or CMC only. The composite hydrogel also showed decreased sensitivity to the ionic strength of water (Fekete et al., 2017). Although physical modifications can improve the polarity and mechanical features of the bio-hydrogel, the chemical crosslinking is needed to prepare a uniform and strong crosslinked network in the hydrogel (Rimdusit, Somsaeng, Kewsuwan, Jubsilp, & Tiptipakorn, 2012; Shahbazi, Ahmadi, Seif, & Rajabzadeh, 2016). Traditional

* Corresponding author at: Department of Natural Resources and Environmental Design, USA. *E-mail address:* lwang@ncat.edu (L. Wang). https://doi.org/10.1016/j.carbpol.2023.121657

Received 25 July 2023; Received in revised form 28 November 2023; Accepted 30 November 2023 Available online 4 December 2023

crosslinkers such as epichlorohydrin and aldehydes (formaldehyde and glutaraldehyde) can significantly improve the mechanical properties and stability of the hydrogel network, but their applications are restricted due to their toxicity. Oxidizing saccharides to polar aldehydes has been considered as promising bio-based crosslinkers with low toxicity and high reaction efficiency (Xu, Canisag, Mu, & Yang, 2015). It has been reported that the oxidation of sucrose could provide the polar functional groups to be comparable with glutaraldehyde in the water stability as a bio-based crosslinker (Liu, Xu, Mi, Xu, & Yang, 2015). Furthermore, oxidized sucrose was reported to show good tensile strength (23 MPa) and tensile strain (60 %) (Xu et al., 2015) compared to other crosslinkers such as epichlorohydrin (50 MPa, 5 %) (Rioux, Ispas-Szabo, Aı¨t-Kadi, Mateescu, & Juhasz, 2002´) and citric acid (24 MPa, 27 %) (Reddy & Yang, 2010), which can be attributed to the high activity of the aldehyde groups (Xu et al., 2015).

This study was to develop a multifunctional, environmentally- friendly iron-enriched biochar and polysaccharide based hydrogel composite that has high conductivity, high porosity and superhydrophilicity to enhance the growth of microalgae. Our research hypothesis was that the novel biochar and hydrogel composite can be slowly degraded in the algal culture to release porous biochar particles enriched with iron and coated with hydrogel to facilitate the attachment and electron mobility of microalgae, and provide a favorable microenvironment with enriched nutrients and CO_2, and iron micronutrient for microalgae growth. **2. Materials and methods**

2.1. Materials

2.1.1. Materials for activated biochar

The corn stover was collected from the North Carolina A&T state university farm (Greensboro, NC, USA). It was dried at 105 °C for 24 h and then grounded to 0.2–0.5 mm particle size and stored at a room temperature. Iron (III) chloride hexahydrate ($FeCl_3{\cdot}6H_2O$), Iron (II) sulfate heptahydrate ($FeSO_4{\cdot}7H_2O$), and sodium hydroxide (NaOH) were purchased from Sigma-Aldrich (St. Louis, MO, USA). Absolute ethanol was purchased from Fisher Chemical.

2.1.2. Materials for hydrogel

Arrowroot starch (MW = 162.14) and Carboxymethyl cellulose (MW = 700,000, DS = 0.9) were purchased from Spectrum Chemical MFG CORP and Acros Organics, respectively. Sucrose and barium chloride anhydrous were purchased from Fisher Chemical. Sodium periodate was purchased from Honeywell.

2.1.3. Chlorella vulgaris

The algal strain was purchased from Carolina Biological Supply Company (North Carolina, USA), was used as a representative microalgal species and maintained in the Bold basal medium. The Bold basal medium contained 25 mg/L $CaCl_2{\cdot}2H_2O$, 75 mg/L $MgSO_4{\cdot}7H_2O$, 250 mg/L $NaNO_3$, 25 mg/L NaCl, 75 mg/L K_2HPO_4, 175 mg/L KH_2PO_4, 50.0 mg/L EDTA, 31.0 mg/L KOH, 4.98 mg/L $FeSO_4{\cdot}7H_2O$, 1 mL/L H_2SO_4, 8.82 mg/L $ZnSO_4{\cdot}7H_2O$, 1.44 mg/L $MnCL_2{\cdot}4H_2O$, 0.71 mg/L MoO_3, 1.57 mg/L $CuSO_4{\cdot}5H_2O$, 0.49 mg/L $Co(NO_3)_2{\cdot}6H_2O$, and 11.42 mg/L H_3BO_3, formulating by deionized water.

2.2. Iron enriched biochar preparation and activation

The biochar was prepared via the slow pyrolysis of corn stover by increasing its temperature to 400 °C at a heating rate of 10 °C/min and maintaining the temperature at 400 °C for 4 h. The carbonization of biomass at 400 °C was reported to generate more O–H and C–H functional groups on the biochar (Angın, 2013).

The biochar was then activated and impregnated by an iron solution, as described in the literature (Yang et al., 2019). The solution was prepared by adding 10 g $FeCl_3{\cdot}6H_2O$ and 5.5 g $FeSO_4{\cdot}7H_2O$ to 300 mL deionized water and stirring at 350 rpm to completely dissolve the iron precursors. 7.7 g biochar was then added to the solution and the mixture was stirred at 350 rpm for 30 min. The pH value was adjusted around 10 by adding 10 M NaOH in drops. The solution was stirred at 350 rpm for 2 h, and then was filtered. The solid residue was washed with water and ethanol and then dried at 70 °C for 12 h. It was reported that drying $Fe(OH)_3$ in the material at a temperature in the range of 40–80 °C could produce the mixture of FeOOH and α-Fe_2O_3 that can be used as an activating agent while only α-Fe_2O_3 would be produced at a temperature above 80 °C (Yang et al., 2019). The dried solid residue was then thermally activated at 400 °C at a heating rate of 10 °C/min for 4 h under purging nitrogen. The activated biochar was washed with water to remove the chemical residues from the surface and dried for 12 h. The yields of biochar from the pyrolysis and activated biochar from the activation were measured at 28.0 % and 93.2 % of input masses.

2.3. Hydrogel preparation

Oxidized sucrose was prepared via the periodate cleavage to be used as a crosslinking agent by following the procedure given in the literature (Xu et al., 2015). Specifically, 6.6 g sucrose and 12.9 g sodium periodate were dissolved in 200 mL of deionized water. The solution was stirred continuously for 26 h. Seven (7) grams of barium chloride was then added to the solution and the mixture was further stirred at 5 °C for 1 h to allow complete precipitation. The mixture was filtered to obtain the liquid containing poly aldehyde derivatives of sucrose. The oxidized sucrose was stored at 5 °C for further use.

CMC and starch were used as basic ingredients to form the 3D structure of the hydrogel. The mass ratio of CMC and starch at 3:1 was used by following the suggestion in the literature (Gayathri & Jayakumari, 2020). The activated biochar impregnated with iron was used as an additive to prepare a nanocomposite hydrogel. Table 1 gives the amounts of ingredients used to prepare various hydrogel samples. H1- H7 samples were prepared to study the effect of various amounts of the crosslinker on the physical and chemical properties of the hydrogel.

For H1–H7 samples, 1.5 g activated biochar and 1 g starch were first added to 100 mL deionized water to form a slurry under stirring at 80 °C for 5 min. Three grams of CMC and 100 mL deionized water were then added gradually into the slurry and stirred at 80 °C for another 2 h. Different amounts of oxidized sucrose (0, 5, 10, 15, 25, 35, and 45 mL) were then added in the 200 mL slurry that was further stirred at 80 °C for another 30 min. The corresponding concentrations of the oxidized sucrose in the slurries were 0.0, 2.4, 4.8, 7.0, 11.1, 14.9, and 18.4 v/v%. After that 1.5 mL glycerol was added and stirred at 80 °C for 10 min. The well mixed slurry was then poured onto glass plates and air-dried for 72 h and then thermally treated in an air oven at 165 °C for 5 min to form a composite hydrogel.

Table 1
The ingredients contents for hydrogel samples preparation.

Sample code	CMC (g)	Starch (g)	Crosslinker (mL)	Glycerol (mL)	Activated biochar (g)
H1	3	1	0	1.5	1.5
H2	3	1	5	1.5	1.5
H3	3	1	10	1.5	1.5
H4	3	1	15	1.5	1.5
H5	3	1	25	1.5	1.5
H6	3	1	35	1.5	1.5
H7	3	1	45	1.5	1.5
H8	3	1	15	2.0	1.5
H9	3	1	15	1.0	1.5
H10	3	1	15	0.5	1.5
H11	3	1	15	1.5	0
H12	3	1	15	1.5	0.5
H13	3	1	15	1.5	1
H14	3	1	15	1.5	2
H15	3	1	0	0	1.5

Samples H8-H10 and H4 were prepared to study the effect of various amounts of glycerol (0.5, 1.0, 1.5, and 2.0 mL) in the slurry at the corresponding concentrations of 0.23, 0.46, 0.69, and 0.92 v/v% on the

properties of the hydrogel. Samples H11-H14 and H4 were prepared to study the effect of various amounts of the activated biochar (0, 0.5, 1, 1.5, and 2 g) in the slurry at the corresponding concentrations of 0.00, 0.25, 0.50, 0.75, and 1.00 w/v% on the properties of the hydrogel. Sample H15 was a mixture of the individual ingredients without any crosslinker and plasticizer at the same mass ratio of 3 CMC : 1 starch: 1.5 activated biochar as Samples H1–H7.

2.4. Biochar and hydrogel characterization

FT-IR spectra of raw biomass, biochar, activated biochar, starch, CMC, and hydrogel were collected at wavenumbers between 400 and 4000 cm^{-1} with a 4 cm^{-1} resolution. FT-IR spectra of sucrose and oxidized sucrose were collected at a 4 cm^{-1} resolution with 64 scans between 400 and 4000 cm^{-1} to see the structural difference after periodate cleavage. The morphology of raw biomass, biochar, activated biochar, and hydrogel was examined using a Zeiss Auriga Field-Emission SEM. The surface area and porosity of raw biomass, biochar, activated biochar, and hydrogel were measured by a BET surface area analyzer (ASAP 2020, Micromeritics, Norcross, GA). The elemental analysis of raw biomass, biochar, and activated biochar was done using a PE 2400 II CHNS/O analyzer (Perkin Elmer, Waltham, MA, USA) and SEM-EDX. The surface elemental composition of the activated biochar was analyzed by using an X-ray photon spectrometer (XPS, Thermo Escalab xi) which was operated under 20 eV passing energy and 0.01 eV step size. Charging correction was done using C1s binding energy of 284.8 eV. The Fisherbrand™ accumet™ XL600 benchtop conductivity meter was employed to measure the electrical conductivity of raw biomass, biochar, activated biochar, and hydrogel. The procedure, as outlined in the literature (Singh, Dolk, Shen, & Camps-Arbestain, 2017), involved combining the samples with deionized water in a 1:10 ratio. The mixture was then mechanically shaken at 25 °C for 1 h at 100 rpm. After a resting period of 30 min, the electrical conductivity (EC) was subsequently measured.

The contact angle of the hydrogel was measured with a dynamic contact angle analyzer (Rame Hart 260-F4, Germany) to determine its hydrophilicity and hydrophobicity (Peng, Ouyang, Deng, Nie, & Kong, 2021). The zeta potential of the hydrogel was measured by dynamic light scattering (DLS, Malvern Instruments ZEN3600) with a concentration of 1 mg/mL. The swelling ratio (SR) of the hydrogels was measured by submerging 0.3 g hydrogel in 100 mL water at a room temperature for 24 h. The mass of the dry hydrogel (m_d) and the mass of the hydrogel after swelling in the water (m_w) were measured. The swelling ratio was calculated by (Lee et al., 2018):

$$SR = (m_w - m_d)/m_d$$

2.5. Enhancement of microalgae cultivation using the composite hydrogel

The primary culture of *C. vulgaris* from the supplier was inoculated into an autoclaved Bold basal medium and subsequently incubated in an incubator shaker (AlgaeTron AG 130-ECO, Quibit systems Inc., Canada) at a light intensity of 100 µE m^{-2} s^{-1} and a temperature of 24 °C for 14 days by following the protocol recommended by the supplier. The pre- cultured *C. vulgaris* was then transferred in a 100 mL tubular photobioreactor (AlgaeTron Multi-Cultivator MC 1000, Brno, Czech Republic) as shown in Fig. 1 using the autoclaved Bold basal medium at the optimal environmental conditions determined by our previous study including light intensity of 240 µEm^{-2} s^{-1}, temperature of 24 °C, and pH of 7.4 (Amini, Wang, & Shahbazi, 2016). Each tubular photobioreactor was filled with 72 mL of fresh Bold basal medium and 8 mL of pre- cultured microalgae at an algae concentration of 13,920 cells/µL. Various amounts of the hydrogel was added to the tubes to obtain its concentrations of 0, 0.625, 1.25, 2.5, 3.75, 6.25 and 12.5 g hydrogel/L culture. The multifunctional hydrogel was initially in the form of a thin film. The hydrogel film was cut into small pieces with various sizes and masses. At the beginning of microalgae cultivation, a piece of hydrogel with a given mass was placed vertically into the tubular photobioreactor with algal culture to obtain the defined concentration. The hydrogel piece gradually descended to the bottom of the photobioreactor. During the cultivation period, the hydrogel piece gradually degraded in the culture to release many small biochar particles enriched with iron and coated with the hydrogel to be used as an additive for the microalgae. For comparison and clarifying the role of 3D cross linker of the hydrogel on algal growth, the original hydrogel ingredients of CMC, starch, and activated biochar at their original powder form were used to prepare a mixture without any cross linker and plasticizer and at the same mass ratio used to prepare the optimum hydrogel (Sample H15), which was used as additives in an algal photobioreactor. Each experiment was repeated three times. Each photobioreactor was bubbled with a gaseous mixture with 5 % CO_2 and 95 % air at a volumetric flow rate of 800 mL/ min.

The dynamic cell concentrations over the 14-day growth period were measured using a flow cytometer (Guava easyCyte™ HT Flow Cytometer, Merck Millipore, Billerica, MA, USA). The pH values of the samples at the end of 14-day growth were measured using a pH meter (accumet XL600, Fisher Scientific, Hampton, NH, USA). The algal culture was centrifuged at 4000 rpm for 20 min to recover the algal cells. Concentrated algal biomass from the centrifugation was then freeze dried. The elemental composition of the dried

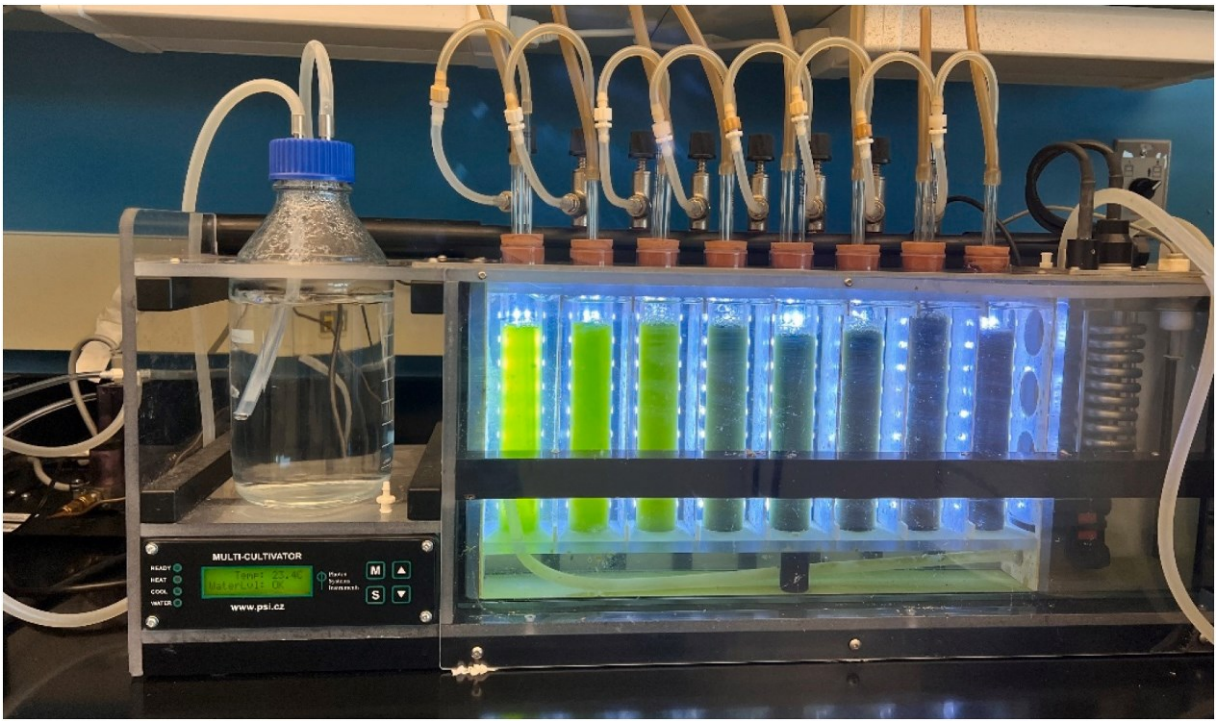

Fig. 1. Multi-tubular photobioreactor (8 tubes) for cultivating microalgae.

algal biomass was analyzed using an elemental analyzer (Perkin-Elmer 2400 CHN/S analyzer, Waltham, MA). The electrical conductivity of the liquid supernatants from the centrifugation was measured using Fisherbrand™ accumet™ XL600 benchtop conductivity meter.

3. Results and discussion

3.1. Structure, physical and chemical properties of the activated biochar

Fig. 2(A) shows the FT-IR spectra of corn stover, its biochar and activated biochar. All these three samples exhibited the same trend in the high frequency regions. The peaks at 3355– 3484 cm^{-1} and 2830–3016 cm^{-1} represented the stretching vibration of the O–H bond, and the C–H bonds of alkanes, respectively, suggesting the presence of –OH and $–CH_3$/$–CH_2$ groups on the surfaces of corn stover, biochar and activated biochar. The pyrolysis and activation slightly shifted and widened the O–H stretching vibration and intensified the C–H bonds of alkanes. The peaks at 1699–1733 cm^{-1} and 1589–1653 cm^{-1} representing C=O and C=C stretching vibrations associated with lignin, respectively, were intensified under the pyrolysis and chemical activation. The peak at approximately 1039 cm^{-1} corresponding to the stretching vibration of C–O due to the presence of hemicellulose, was reduced under the pyrolysis and activation (Peng et al., 2021). The peaks at 580 and 640 cm^{-1} of the activated biochar's spectrum attributing to the Fe–O stretching vibration and Fe–OH bending vibrations (Yang et al., 2019), confirmed the existence of α-Fe_2O_3 and α-FeOOH on the surface of the activated biochar.

Fig. 2(B) shows the XPS spectrum of Fe 2p for Fe–O and Fe_2O_3 of the activated biochar. The peaks of Fe $2p_{3/2}$, Fe $2p_{1/2}$ and Fe $2p_{3/2}$ satellite for Fe–O were 710.52 ± 0.16, 724.44 ± 0.11 and 714.95 ± 0.27 eV, respectively. These peaks well matched with the reported binding energies for the Fe–O standard sample at 709.5 ± 0.02 eV for Fe $2p_{3/2}$, 723.2 ± 0.05 eV for Fe $2p_{1/2}$, and 715.5 ± 0.05 eV for Fe $2p_{3/2}$ satellite (Yamashita & Hayes, 2008). The peaks at 712.05 ± 0.21 eV and 719.39 ± 0.17 eV were attributed to the Fe $2p_{3/2}$ and its satellite for Fe_2O_3, respectively, which agreed with the reported peaks for Fe_2O_3 in literature, suggesting the range of 710.6–711.2 eV for the position of the Fe $2P_{3/2}$ peak and approximately 8 eV higher than the main Fe $2P_{3/2}$ peak for the Fe $2P_{3/2}$ satellite of Fe_2O_3. The peak at 727.81 ± 0.13 eV was attributed to the Fe $2P_{1/2}$ peak for Fe_2O_3. Moreover, the peak at 732.96 ± 0.11 eV was probably attributed to the satellite peak of Fe $2p_{1/2}$ (Yamashita & Hayes, 2008). Therefore, both the XPS and FT-IR spectrums showed the presence of Fe_2O_3 and Fe–OOH in the samples.

Table 2 gives the physical properties of the raw corn stover, its biochar and activated biochar. The BET surface areas of raw corn stover, biochar and activated biochar were 1.33, 2.58, and 47.52 m^2/g, respectively. Pyrolysis and subsequent activation increased the BET surface area of corn stover by 1.94 and 35.78 times, respectively. The pore volume of corn stover also increased by 1.5 times during carbonization and 53.25 times during activation.

As shown in Table 2, the pyrolysis of corn stover increased its carbon content from 55.55 % to 75.95 %. Meanwhile, the pyrolysis decreased

Table 2
Properties and elemental compositions of corn stover, biochar, and activated biochar.

Properties	Corn stover	Biochar	Activated biochar
pH	5.62	8.89	10.5
Electrical conductivity (mS/cm)	2.89	3.82	4.67
BET surface area (m^2/g) Pore	1.328	2.581	47.517
volume (cm^3/g)	0.004	0.006	0.213
Pore width (nm)	12.601	9.199	17.89
C %	55.55	75.95	50.45
O %	40.90	15.45	19.65
Fe %	0	0	27.25

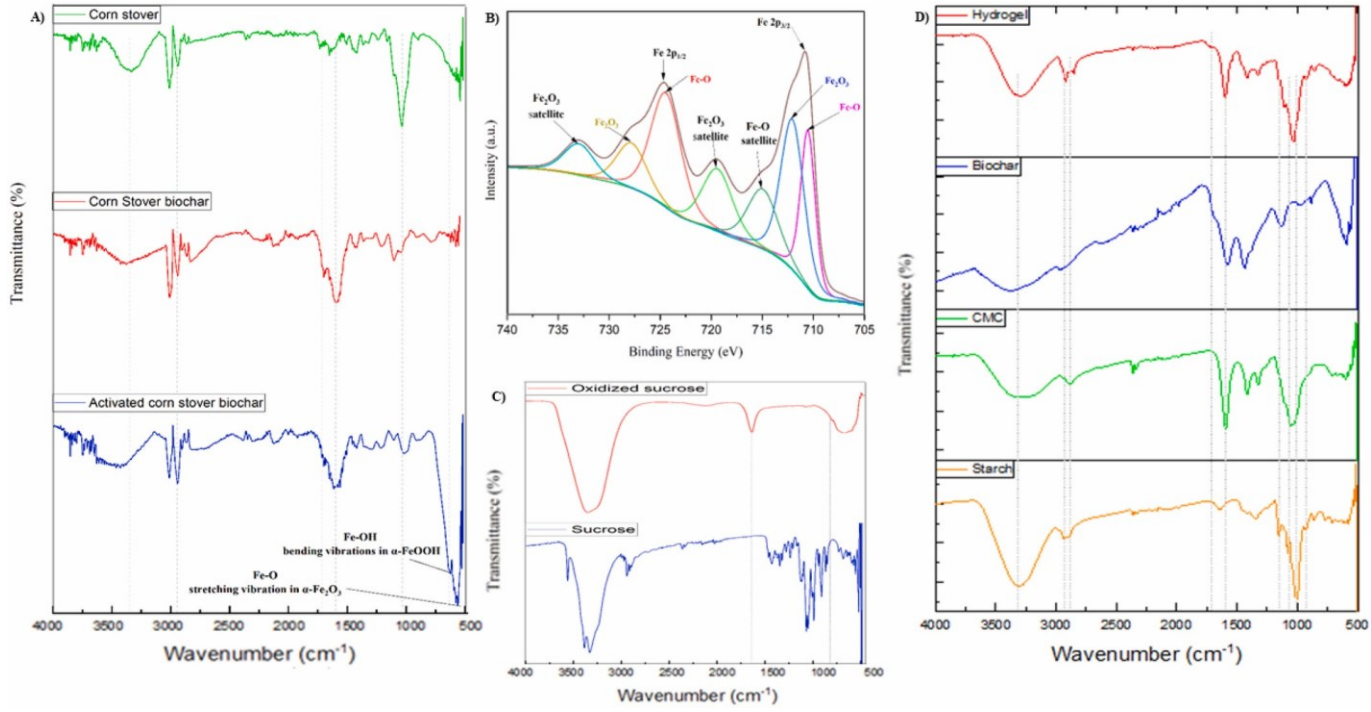

Fig. 2. A) FT-IR spectra of corn stover, biochar, and activated biochar; B) XPS spectrum of Fe 2p for Fe_2O_3 and Fe–O of the activated biochar; C) FT-IR spectra of sucrose and oxidized sucrose; and D) FT-IR spectra of CMC, starch, activated biochar, and hydrogel.

K%	1.2	3.4	0.1
Si %	1.05	1.2	1.7
Cl %	0.6	0.85	0.1
Ca %	0.3	1.3	0.25
Mg %	0.2	0.75	0
P %	0.1	0.7	0.2
S %	0.1	0.3	0.2
Al %	0.1	0.1	0.1
H% (Elemental analyzer's result)	6.69	2.60	1.26

oxygen content from 40.90 % to 15.45 %, and hydrogen content from 6.69 % to 2.60 %. As the H/C and O/C atomic ratios were decreased from 0.12 to 0.03, and 0.74 to 0.2 by the pyrolysis, respectively, the biochar had more aromatic and carbonaceous structure than the raw biomass (Angın, 2013). Iron impregnation and activation of the biochar not only increased the pH value from 8.89 to 10.5, but also increased the iron content from 0 % in the biochar to 27.25 % in the activated biochar, and electrical conductivity from 3.82 mS/cm for the biochar to 4.67 mS/ cm for the activated biochar. The activation of biochar using an iron solution reacted with NaOH could introduce iron oxide functional groups into the biochar to partially decomposes the structure of the biochar. The subsequent thermal activation could further release volatiles to produce many small pores in the biochar (Sakhiya, Anand, & Kaushal, 2020; Yang et al., 2019). The carbonization and activation with an iron solution significantly increased the BET surface area, porosity, iron content, and electrical conductivity of the biochar.

Fig. 3(A–F) shows the SEM and the EDX images of the corn stover, biochar and activated biochar. Fig. 3(A–C) show that there was a significant difference in porous structures and surface morphologies among the raw biomass, biochar, and activated biochar. The SEM image of the activated biochar with higher magnification (23,000×) given in Fig. 3 (D) clearly shows that the iron particles were impregnated on the surface of activated biochar at nano scales.

The SEM-EDX layered images given in Fig. 3(E) and (F) further show that the iron nanoparticles were distributed on the surface of the activated biochar.

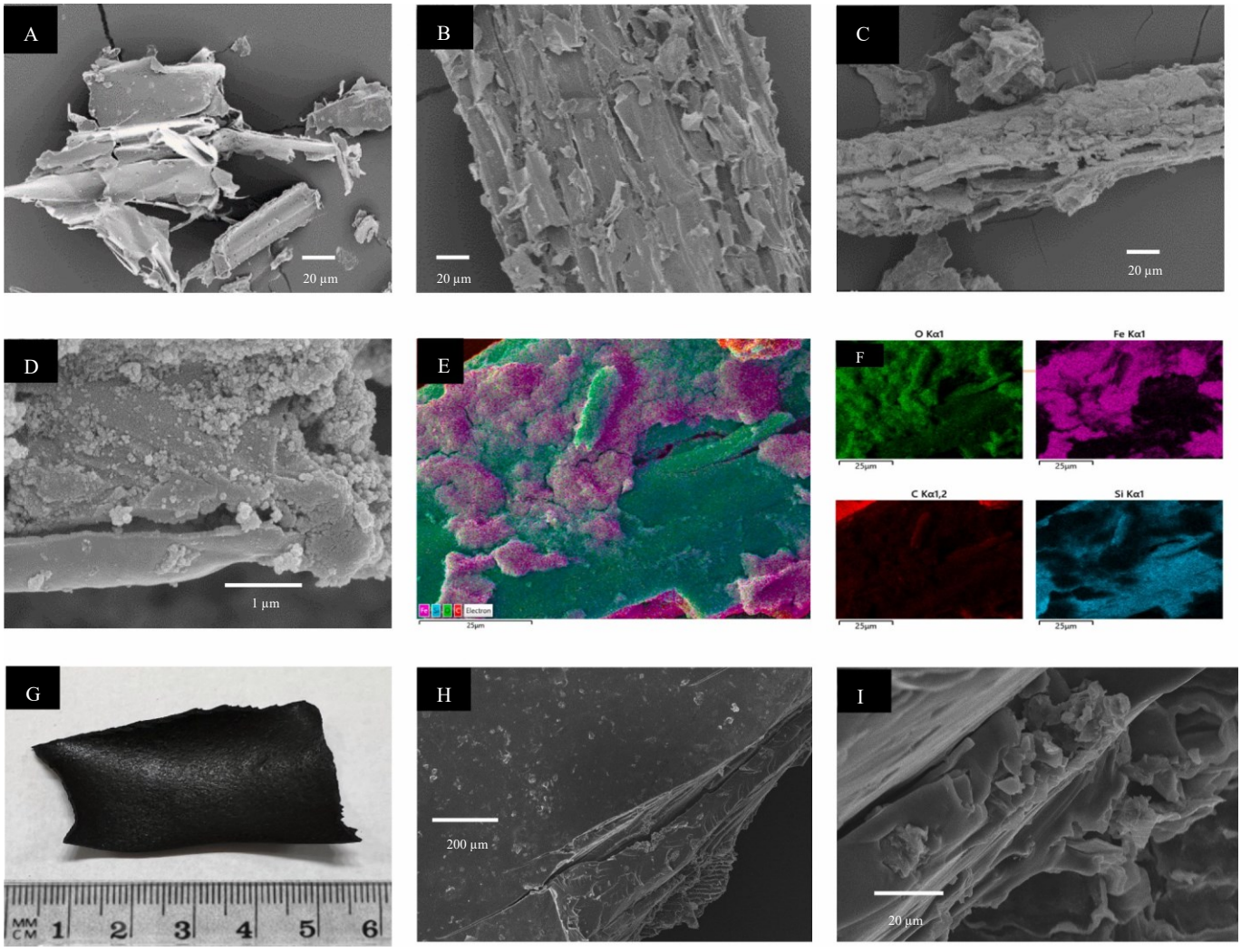

Fig. 3. SEM images of corn stover (A), biochar (B), activated biochar (C), activated biochar (23,000×) (D), and EDX layered images (E) and (F). The macroscopic image of the hydrogel (G) and FE-SEM images of the hydrogel at 100× (H) and 1010× magnifications (I).

3.2. Physical and chemical properties of the hydrogel

3.2.1. Oxidized sucrose characteristics

In order to confirm the periodate oxidation of sucrose, the FT-IR spectra of sucrose and oxidized sucrose were compared. As shown in Fig. 2(C), sucrose and oxidized sucrose contain a broad band at around 3345 cm^{-1} indicating the presence of hydroxyl group in the structure which is stronger and broader at oxidized sucrose than sucrose. The main difference between sucrose and oxidized sucrose is the presence of the band at 1643 cm^{-1} at oxidized sucrose spectrum attributing to the unsaturated aldehyde group which confirms the periodate oxidation of sucrose and presence of aldehyde groups (Feng et al., 2022; Xu et al., 2015). Furthermore, the presence of a weak peak at 808 cm^{-1} in oxidized sucrose can be assigned to the formation of hemiacetal bonds between aldehyde groups and neighbor hydroxyl groups (Lee et al., 2018).

3.2.2. Effect of the crosslinking agent

The crosslinking agent increased the resistance of the hydrogel to be dissolved in water by enhancing intra-structure chemical interactions to form a strong 3D network. However, the use of too many crosslinkers decreases the porosity of the hydrogel, leading to a reduction in water adsorption capacity and the swelling ratio (Canisag, 2015; Xu et al., 2015). Fig. 4 shows the effects of different amounts of the crosslinker (0, 2.4, 4.8, 7.0, 11.1, 14.9 and 18.4 v/v %) on the swelling ratio and BET surface area of the hydrogel. Without a crosslinker, the network of CMC, starch, and activated biochar in the hydrogel swelled very fast and were dissolved completely in water after a short period of time. The crosslinker affected the stability, porosity, and hydrophilicity of the hydrogel.

As shown in Fig. 4(A), when the concentration of the crosslinker of oxidized sucrose increased from 0 to 2.4 % (v/v), the swelling ratio increased from 58.69 to 65.06 (g/g) and meanwhile the BET surface area increased by 1.69 times as shown in Fig. 4(B). The further increase of the crosslinker content to 7.0 % (v/v) not only increased the stability of the hydrogel in the water by enhancing the chemical interaction among ingredient polymers, but also increased the swelling ratio to 63.33 g/g due to the increase of the hydrophilicity of the network. However, the further increase of the crosslinker content not only decreased the water stability of the hydrogel, but also noticeably decreased its swelling ratio attributing to the increased hydrophilicity and reactivity, and decreased porosity and BET surface area of the 3D network. As shown in Fig. 4(B), the increase of the crosslinker's content to 18.4 % decreased the BET surface area to 0 m^2/g. The increases of the crosslinker content from 0 % to 18.4 % increased the electrical conductivity of the hydrogel from 0.32 to 1.40 mS/cm (Fig. 4(C)) and decreased the pH from 7.71 to 5.63 (Fig. 4 (D)) due to the increase of the hydrogel density and the addition of more acidic functional groups, respectively. By considering the swelling ratio, water stability, specific surface area and electrical conductivity, 7 % (v/ v) was considered as the optimum concentration of the oxidized sucrose crosslinker for preparing the hydrogel which was in line with the results reported in literature (Canisag, 2015; Xu et al., 2015).

Previous studies have shown that the attachment of microalgae onto porous supports significantly enhances their growth by promoting biofilm formation and enriching nutrients via adsorption (Kholssi et al., 2018; Mashkour, Rahimnejad, & Mashkour, 2016). The porosity and surface chemistry of the supports affect their ability to create a favorable micro-environment to facilitate the attachment of microorganisms and nutrient adsorption. High specific surface area and porosity of the activated biochar improve the adsorption of nutrients and CO_2 and promote algal biofilm formation. The biochar enriched with iron can also slowly release iron nanoparticles as essential micronutrient for the microalgae growth. In this study, an iron solution was used to simultaneously activate biochar and enrich its iron content. Furthermore, the iron on the biochar increased the electrical conductivity of the biochar particles, which can facilitate efficient electron transfer for the metabolic processes of microalgae including photosynthesis and respiration (Vargas-Estrada et al., 2020).

A piece of hydrogel-biochar-iron composite that was introduced to the algal culture gradually degraded to release many small iron-rich biochar particles coated with the hydrogel. Those biochar-hydrogel particles are used as a support for attached microalgae growth. The hydrogel with a higher swelling ratio coated on the surface of biochar has a greater capacity to retain water and nutrients and provide a better scaffold for the microalgae to develop biofilm.

3.2.3. Effect of the plasticizer

The interaction between starch and CMC chains has the tendency to form a brittle structure. Plasticizers such as glycerol can be added to enhance the mobility and flexibility of the crosslinked network of the hydrogel via interfering with polymeric chains (Canisag, 2015; Xu et al., 2015). Fig. 5 shows the effects of various amounts of glycerol at 0.23, 0.46, 0.69, and 0.92 % (v/v)

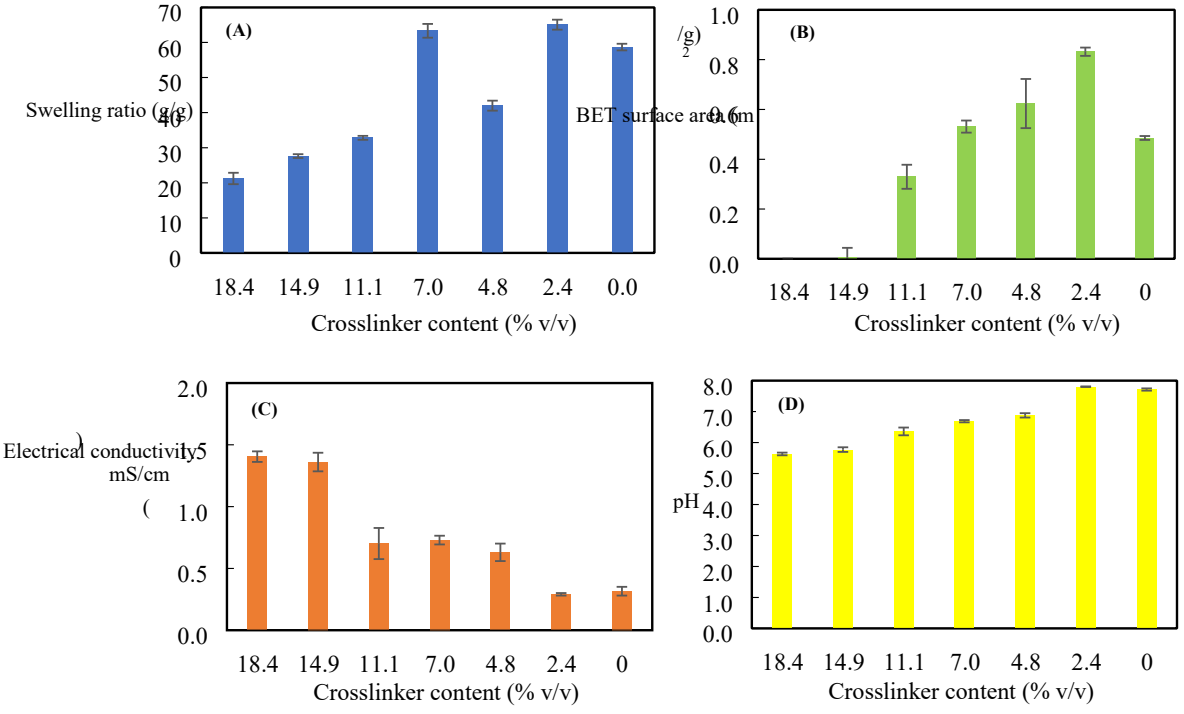

Fig. 4. Effect of the crosslinker (oxidized sucrose) content on the swelling ratio (A), porosity (B), EC (C), and pH (D).

added to the 200 mL hydrogel slurry with 1 g starch, 3 g CMC, 1.5 g activated biochar, and 15 mL crosslinker on the swelling ratio of the hydrogels.

The increase of the glycerol content from 0.23 % to 0.69 % increased the swelling ratio from 44.52 to 63.33 g/g. The further increase of the glycerol content to 0.92 % (v/v) sharply decreased the swelling ratio to 42.48 g/g due to the decreased strength of the crosslinked network and the increased dissolution of the polymers in water. Therefore, the optimum concentration of glycerol for preparing the hydrogel was found to be 0.69 % (v/v). The amount of 1.5 mL glycerol used in this study was about 35 % of the total mass of polymers (1 g starch, 3 g CMC, and 1.5 g activated biochar), which was higher than 15 % of the mass of starch as the optimum glycerol concentration reported in the literature (Xu et al., 2015). The higher content of glycerol used in the current study might be attributed to the use of different polymers.

3.2.4. Effect of activated biochar additive

Fig. 6 shows the effects of different amounts of the activated biochar (0, 0.25, 0.50, 0.75, and 1.0 (w/v) %) on the swelling ratio, porosity, and electrical conductivity of the hydrogel. The addition of the activated biochar to the hydrogel increased the porosity and electrical conductivity of the hydrogel. It can be seen in Fig. 6(A–B) that the addition of 1.0 wt% of the activated biochar to the hydrogel slurry remarkably increased the electrical conductivity and BET surface area of the hydrogel by 3.05 and 3.84 times, respectively, compared to the hydrogel without the activated biochar. The increase of the biochar content from 0 to 0.75 % increased the swelling ratio of the hydrogel by 4.91 times (Fig. 6(C)), which was attributed to the added porosity of the biochar. The further increase of the biochar content to 1 % decreased the swelling ratio to 53.92 g/g as too much biochar weakened the 3D crosslinking network and water uptake capacity of the hydrogel. Therefore, the optimum concentration of the activated biochar for preparing the hydrogel was found to be 0.75 (w/v) %, which increased the BET surface area and electrical conductivity of the hydrogel by 2.80 and 2.29 times, respectively compared to the hydrogel without the biochar.

3.2.5. Hydrogel morphology

Fig. 3(G–I) shows the macroscopic and microscopic surface morphology of the hydrogel with the optimum contents of 7 (v/v) % oxidized sucrose as a crosslinker, 0.69 (v/v) % glycerol as a plasticizer and 0.75 (w/v) % activated biochar during the preparation of the hydrogel. As shown in Fig. 3(G), the color of the hydrogel was black due to the presence of activated biochar. The dry hydrogel was a strong thin film with low flexibility. The wrinkles and pores on the surface of the hydrogel as shown in Fig. 3(H) could facilitate water permeation into the network through interaction between their hydrophilic functional groups and water molecules (Lee et al., 2018). Fig. 3(I) shows that the hydrogel had a porous morphology with a broad network structure that could retain a large amount of water. The pH of the hydrogel was 6.69 ± 0.04 which was consistent with a negative zeta potential (− 30.4 ± 2.48 mV) due to the presence of slight negative charge on the surface of hydrogel.

Fig. 2(D) shows the FT-IR spectra of the hydrogel and its main ingredients of CMC, starch, and activated biochar. The starch spectrum exhibits peaks at 3315 and 2927 cm^{-1}, corresponding to the stretching vibration of –OH and C–H, respectively (Gayathri & Jayakumari, 2020). Additionally, several discernible peaks at 1151, 1079, 1008 and
925 cm^{-1} were assigned to the C–O bond stretching (Gayathri & Jayakumari, 2020; Lee et al., 2018). The peaks at 1079 and 1008 were reported as the characteristics of C–O stretching in anhydroglucose ring (Lee et al., 2018). In the CMC spectrum the peaks at 3276 cm^{-1}, 2923 cm^{-1}, and 1592 cm^{-1} were observed, corresponding to the OH group, C–H bond, COO– (carboxyl) group, respectively. A vibrational stretching peak at 1041 cm^{-1} also represented the C–O–C group in CMC (Gayathri & Jayakumari, 2020). The peaks at 3484, 3014, 1699, and 1589 cm^{-1} in the activated biochar spectrum were assigned for –OH and C–H stretching, COO– asymmetric of carboxylic acid, respectively. Hydrogel spectrum by representing almost all characteristic peaks of its ingredients confirmed the compatible bonding and physical crosslinking among starch, CMC and activated biochar (Gayathri & Jayakumari, 2020). Under crosslinking, the peak at 925 cm^{-1} in the starch spectrum was weakened in hydrogel spectrum, and C–O stretching at 1151 and 1079 cm^{-1} were replaced by a new peak at 1105 cm^{-1} due to the C–O ether and C–O–C acetal bridge formation, which confirmed the chemical crosslinking between aldehyde groups in oxidized sucrose and hydroxyl groups in other ingredients. Moreover, the presence of peaks at 1590 and 1720 cm^{-1} for the carboxyl and aldehyde groups also shows the probable crosslinking between the hydroxyl group in CMC, starch and activated biochar, and the aldehyde group in oxidized sucrose, caused the loss of the aldehyde groups and formation of new C–O–C etheric groups in hydrogel (Lee et al., 2018). The measured average contact angle between water drops and hydrogel surface was 58 ± 1.9°, which further confirmed the hydrophilicity of the hydrogel's surface.

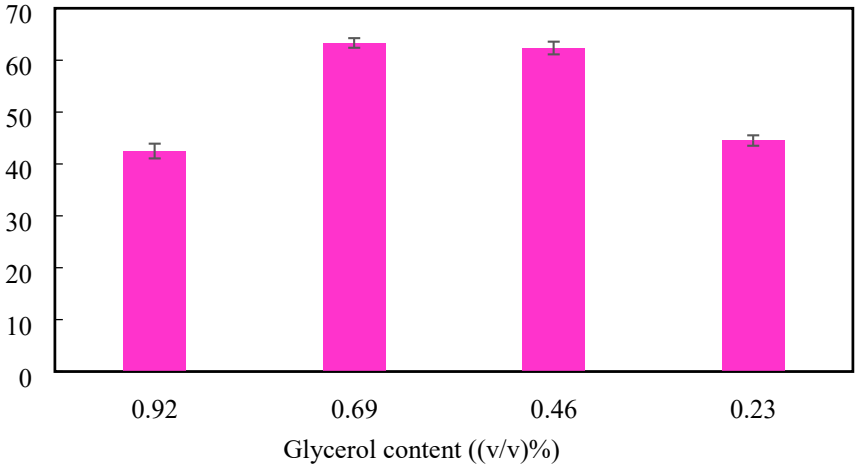

Fig. 5. Effect of the plasticizer (glycerol) content on the swelling ratio.

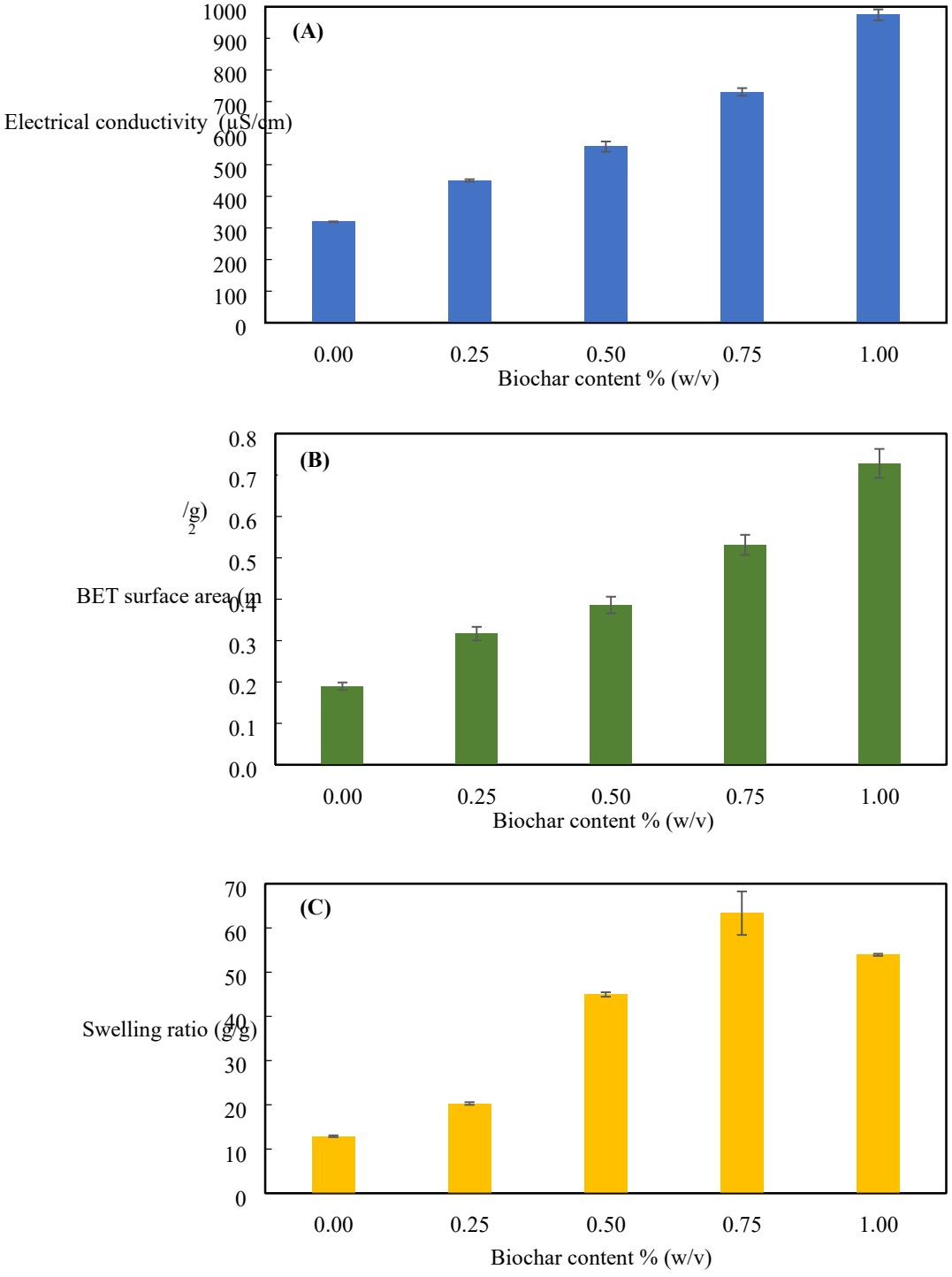

Fig. 6. Effect of activated biochar content on electrical conductivity (A), BET surface area (B), and swelling ratio of the hydrogel (C).

3.3. Enhancement of microalgae growth using the hydrogel

3.3.1. Effects of the hydrogel additive on the algal yield, cell concentration, and elemental composition

Fig. 7(A) shows the growth curves of microalgae cultivated with different amounts of hydrogel. It can be seen from Fig. 7(A) that the introduction of the hydrogel additive into the algal culture decreased the algal growth during the lag phase. However, the hydrogel additive at an optimum amount which was obtained at 2.5 g/L could significantly enhance the microalgae growth during the exponential growth phase. The hydrogel additive at its optimum amount could also increase the exponential growth period.

Fig. 7(B) and (C) show the effects of different amounts of hydrogel on the algae yield and cell concentration over a 14-day cultivation period. The maximum algae yield, and cell concentration were obtained by adding 2.5 g/L hydrogel. As shown in Fig. 7(B) and (C), the algae yield and cell concentration in the culture containing 2.5 g/L hydrogel increased by 65.7 % and 92.2 %, respectively, compared to those in the control culture without hydrogel. However, the further increase of the hydrogel content decreased the algae

yield and cell concentration. If the hydrogel content further increased to 12.5 g/L, the algae yield and cell concentration decreased by 19 % and 67.8 %, compared to the control.

Fig. 7. Microalgae growth with different contents of the hydrogel: dynamic growth curves (A), biomass yield after 14-day growth (B), cell concentration after 14-day growth (C).

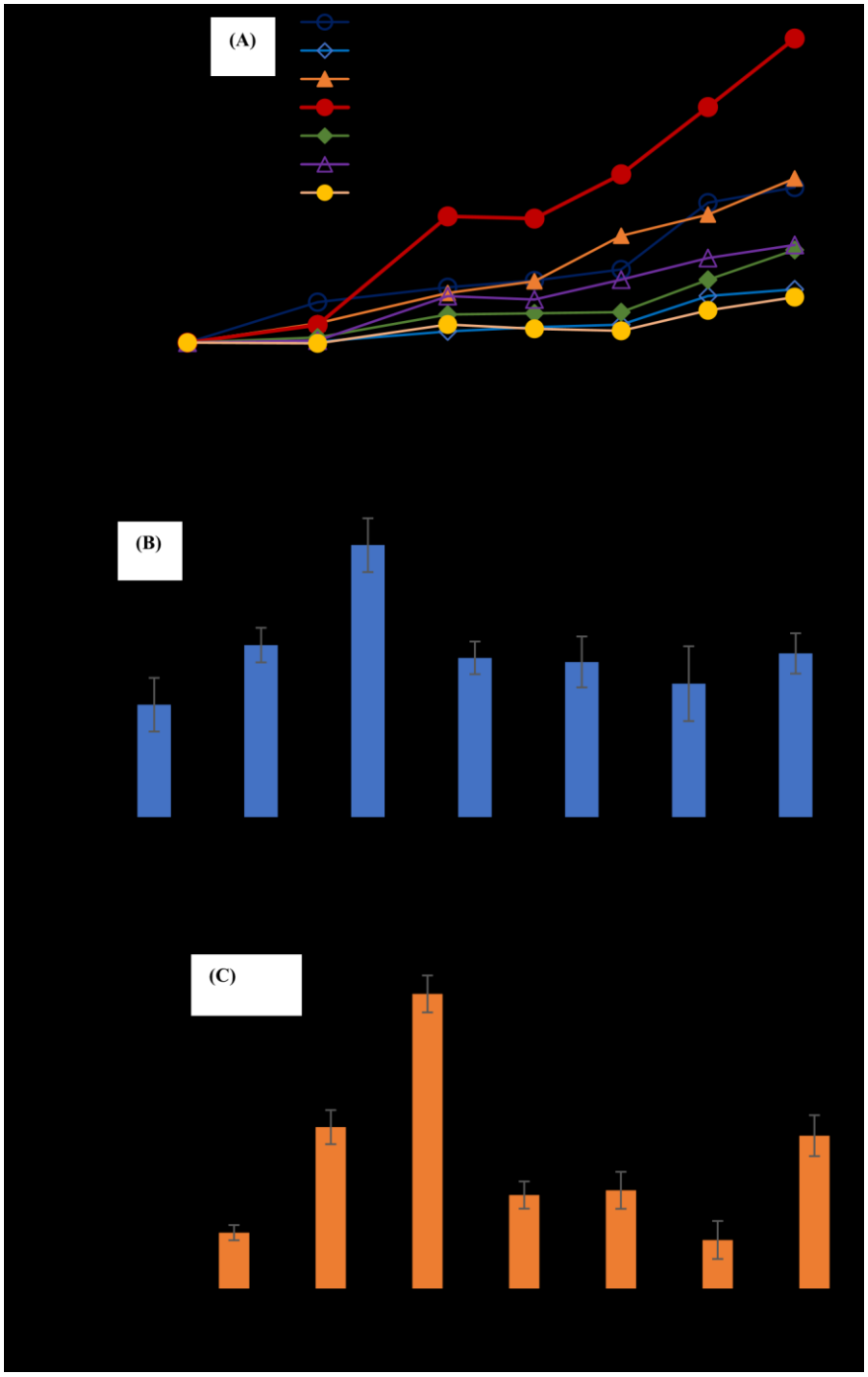

The improvement of algal growth with the hydrogel additive may be attributed to the two mechanisms of hydrogel. First, the hydrogel composite can slowly release iron as an essential micronutrient to promote the cellular functions of microalgae like photosynthesis and respiration (Salehi & Wang, 2022; Vargas-Estrada et al., 2020). Second, the composite can serve as a conductive scaffold for attached microalgae cultivation by creating a desirable microenvironment with enriched CO_2 and nutrients through an adsorption/desorption cycle (De Morais, Vargas, da Silva Vaz, Cardias, & Costa, 2021), and improved light harvesting and usage efficiency through the interaction between the light and the conducting electrons of iron nanoparticles (Eroglu, Eggers, Winslade, Smith, & Raston, 2013; Torkamani, Wani, Tang, & Sureshkumar, 2010). However, the effectiveness depends on the hydrogel and iron concentration in the culture medium and their synergy or antagonistic effect with other environmental factors (Sajjadi, Chen, Raman, & Ibrahim, 2018).

Too high concentration of hydrogel (higher than 2.5 g/L) negatively affected the algal growth, which might be attributed to the generation of various reactive oxygen species (ROS) via Fenton-type reactions that cause oxidative injury to cells via lipid peroxidation and oxidation of thiol groups on proteins and DNA (LeBel, Ischiropoulos, & Bondy, 1992). ROS generation can be correlated with the increase in electrical conductivity. As shown in Fig. 8, the increase of the hydrogel content significantly increased the electrical conductivity of the culture medium due to the release of the irons from the hydrogel. The electrical conductivity of the culture medium with 2.5 g/L hydrogel was 1.32 mS/cm, compared to 0.75 mS/cm for the control culture without the hydrogel. If the hydrogel content further increased to 12.5 g/L, the electrical conductivity increased to 2.39 mS/cm. There is an optimum iron content or electrical conductivity to enhance the algae growth.

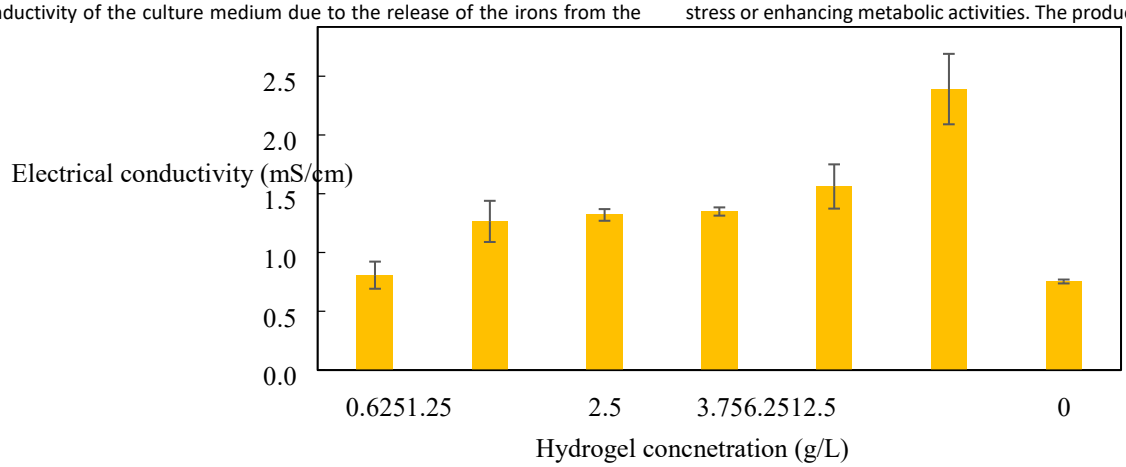

Fig. 8. Electrical conductivity of the algal culture medium with different hydrogel contents.

Fig. 9 shows the impact of hydrogel on the elemental composition of microalgae. If 2.5 g/L hydrogel was added to the culture to obtain the maximum algae yield and cell concentration, the contents of carbon, hydrogen, nitrogen, and sulfur of the algae were 50.01 %, 7.14 %, 2.70 %, and 1.66 %, compared to 50.64 %, 8.26 %, 2.23 %, and 1.53 % in the control culture without hydrogel. Therefore, the addition of small amount of hydrogel (i.e., 2.5 g/L) significantly decreased the hydrogen content (by 13.6 %) and increased the nitrogen content (by 21.1 %) of the algae. If the hydrogel content further increased to 12.5 g/L, the contents of carbon, hydrogen, and sulfur decreased to 30.63 %, 3.72 %, and 1.08 % while the nitrogen content increased to 3.05 %. The addition of 6.25 g/L hydrogel achieved the highest nitrogen content of 4.14 wt%, compared to 2.23 wt% in the control sample.

The algal biomass also contains a large amount of oxygen, which is usually determined as 100 %-C%-H%-N%-S%, and traceable amounts of minerals such as Fe, and P. The oxygen contents slightly increased with the addition of hydrogel. Nitrogen is a crucial element for cellular processes, particularly in the synthesis of proteins, nucleic acids, and other essential molecules. It plays a central role in the growth and function of the cells. When algae experience stress with the hydrogel additive enriched with iron at a high amount, they may uptake more nitrogen to support the production of N-containing compounds to deal with the environmental stress. The increase in the N content can be seen as a compensatory mechanism. Algae may prioritize the maintenance of critical cellular processes, such as repairing damage caused by stress or enhancing metabolic activities. The production of more N-containing compounds such as proteins can affect the overall elemental composition of the algal cells.

3.3.2. Effect of crosslinked network of hydrogel on the microalgae growth In order to analyze the impact of introducing activated biochar, CMC, and starch in the form of hydrogel to microalgae culture, the microalgae growth in the presence of 2.5 g/L hydrogel which offered the highest biomass yield and cell concentration, was compared with a culture containing the proper amounts of individual raw hydrogel ingredients without the crosslinker. As shown in Fig. 10, both the hydrogel and the mixture of the ingredients of CMC, starch, and activated biochar could significantly increase the algae yield and cell concentration. The algae yield and cell concentration in the culture with the ingredient mixture increased by 45.4 % and 74.0 %, respectively, compared to those of the control. However, the corresponding hydrogel had better performance than the mixture of the same amounts of individual hydrogel ingredients.

As shown in Fig. 10, the biomass yield and cell concentration in the culture with 2.5 g/L hydrogel improved by 13.9 % and 10.5 %, respectively, compared to those of the algae in the culture with the ingredient mixture. This might be attributed to the ability of the hydrogel to serve as a better conductive scaffold by slowly releasing

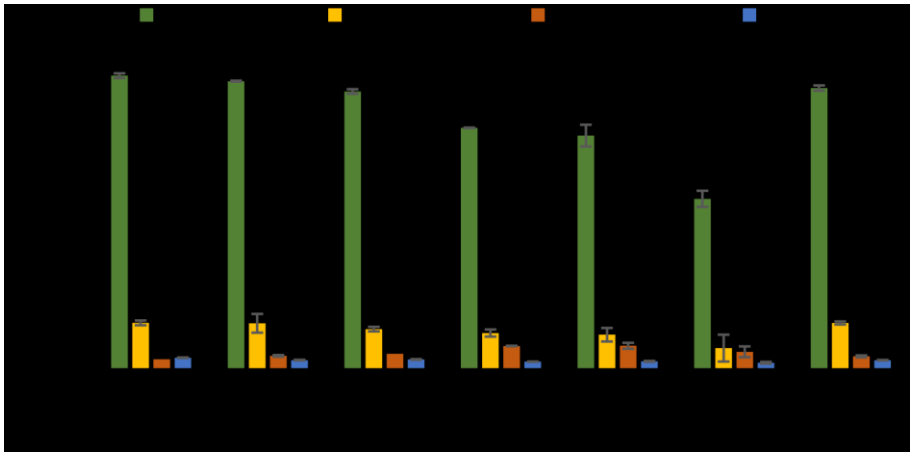

Fig. 9. Elemental composition of microalgae cultivated with different contents of the hydrogel.

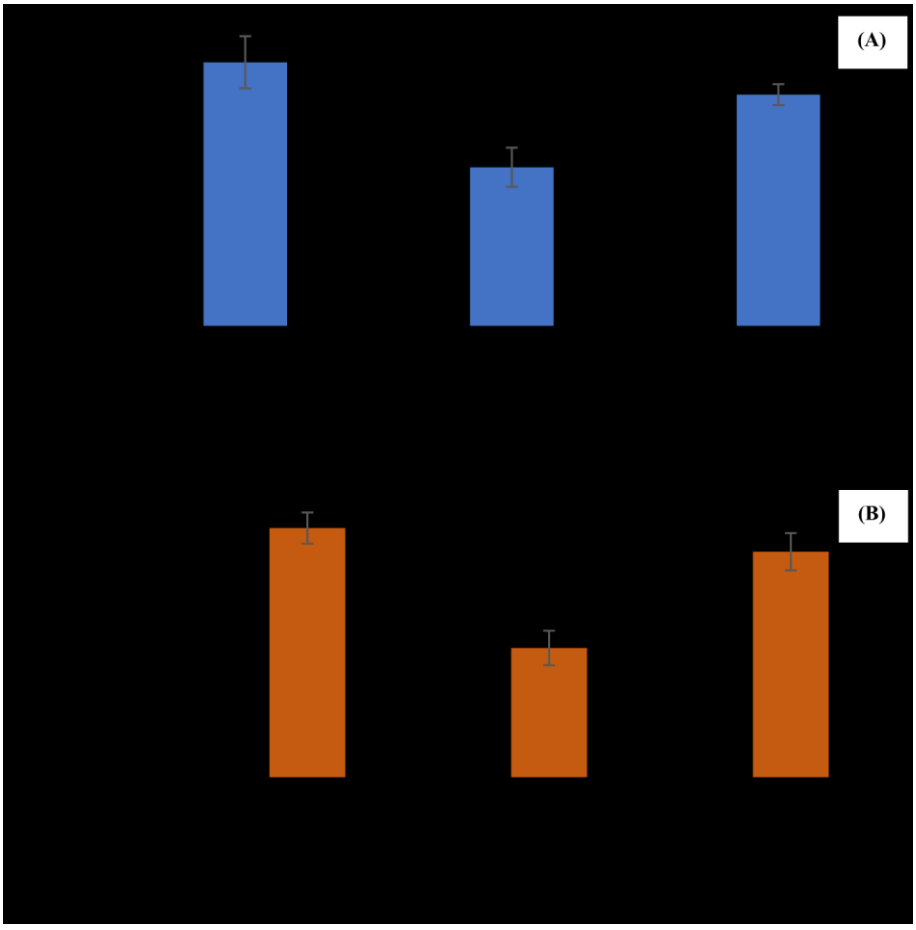

Fig. 10. Comparison of the addition of hydrogel and non-crosslinked hydrogel ingredients on the algal biomass yield (A) and cell concentration (B).

activated biochar particles enriched with iron and coated with the hydrogel for attached microalgae growth.

The hydrogel structure was designed to serve as a mini-scaffold for microalgal attachment, growth and harvesting, and an adsorbent to enrich nutrients and CO_2 in the culture. The hydrogel-biochar composite was prepared by using cost-effective renewable ingredients of polysaccharides of lignocellulosic biomass and starch through a biobased crosslinker of oxidized sucrose. Therefore, there is no need to separate microalgal biofilm on the hydrogel support after harvesting. Considering the low cost of ingredients and cross linker for preparing the hydrogel, low dosage used in algal cultivation, and multi-functionalities for enhancing algal growth, the hydrogel is a promising economic and sustainable additive to be used for enhancing algal growth and harvesting.

4. Conclusions

A multifunctional hydrogel was synthesized by crosslinking activated biochar, CMC and starch with a bio-crosslinker of oxidized sucrose and plasticizer of glycerol to enhance algal production. The activation and impregnation of biochar with $FeCl_3{\cdot}6H_2O$ and $FeSO_4{\cdot}7H_2O$ increased its conductivity by 22.25 % and BET surface area by 1741.03 %. The algal yield and cell concentration after 14 days of growth in a Bold basal medium with an optimum concentration of 2.5 g hydrogel/L increased by 65.7 % and 92.2 %, respectively, compared to these of the control without the hydrogel. The further increase of hydrogel concentration decreased algal yield and cell concentration. The hydrogel additive could significantly increase the nitrogen content but decrease the carbon, hydrogen, sulfur contents of the microalgae. The algal yield and cell concentration in the culture with 2.5 g/L hydrogel improved by 13.9 % and 10.5 %, respectively, compared to those of the algae in the culture with the same amounts of individual non–crosslinked hydrogel ingredients.

CRediT authorship contribution statement

Bahare Salehi: Writing – original draft, Visualization, Validation, Methodology, Investigation, Formal analysis, Data curation, Conceptualization. **Bo Zhang:** Methodology. **Kyle Nowlin:** Methodology. **Lijun Wang:** Writing – review & editing, Supervision, Resources, Project administration, Methodology, Funding acquisition, Formal analysis, Data curation, Conceptualization. **Abolghasem Shahbazi:** Resources.

Declaration of competing interest

The authors declare the following financial interests/personal relationships which may be considered as potential competing interests: Lijun Wang reports financial support was provided by US Department of Agriculture. Lijun Wang reports financial support was provided by US Department of Energy.

Data availability

Data will be made available on request.

Acknowledgment

This research was supported by funds provided by US Department of Agriculture - National Institute of Food and Agriculture (Grant #: NC.X 345-5-22-130-1) and US Department of Energy (Grant #: EE0008809).

References

Amini, H., Wang, L., & Shahbazi, A. (2016). Effects of harvesting cell density, medium depth and environmental factors on biomass and lipid productivities of Chlorella vulgaris grown in swine wastewater. *Chemical Engineering Science, 152*, 403–412.

Angın, D. (2013). Effect of pyrolysis temperature and heating rate on biochar obtained from pyrolysis of safflower seed press cake. *Bioresource Technology, 128*, 593–597.

Ansah, E., Wang, L., Zhang, B., & Shahbazi, A. (2018). Catalytic pyrolysis of raw and hydrothermally carbonized Chlamydomonas debaryana microalgae for denitrogenation and production of aromatic hydrocarbons. *Fuel, 228*, 234–242.

Canisag, H. (2015). *Bio-crosslinking of starch films with oxidized sucrose*.

Chen, Y.-C., & Chen, Y.-H. (2019). Thermo and pH-responsive methylcellulose and hydroxypropyl methylcellulose hydrogels containing K_2SO_4 for water retention and a controlled-release water-soluble fertilizer. *Science of the Total Environment, 655*, 958–967.

Cui, C., Jia, Y., Sun, Q., Yu, M., Ji, N., Dai, L., … Sun, Q. (2022). Recent advances in the preparation, characterization, and food application of starch-based hydrogels. *Carbohydrate Polymers, 291*, Article 119624.

Das, S. K., Ghosh, G. K., & Avasthe, R. (2021). Applications of biomass derived biochar in modern science and technology. *Environmental Technology & Innovation, 21*, Article 101306.

De Morais, M. G., Vargas, B. P., da Silva Vaz, B., Cardias, B. B., & Costa, J. A. V. (2021). Advances in the synthesis and applications of nanomaterials to increase CO_2 biofixation in microalgal cultivation. *Clean Technologies and Environmental Policy*, 1–16.

Eroglu, E., Eggers, P. K., Winslade, M., Smith, S. M., & Raston, C. L. (2013). Enhanced accumulation of microalgal pigments using metal nanoparticle solutions as light filtering devices. *Green Chemistry, 15*(11), 3155–3159.

Fekete, T., Borsa, J., Takacs, E., & Woj´ narovits, L. (2017). Synthesis of´ carboxymethylcellulose/starch superabsorbent hydrogels by gamma-irradiation. *Chemistry Central Journal, 11*, 1–10.

Feng, M., Hu, X., Yin, Y., Liang, Y., Niu, J., & Yao, J. (2022). Structural analysis of oxidized sucrose and its application as a crease-resistant crosslinking agent. *Polymers, 14*(14), 2842.

Gayathri, D., & Jayakumari, L. S. (2020). Evaluation of commercial arrowroot starch/ CMC film for buccal drug delivery of glipizide. *Polímeros, 29*, Article e2019047.

Karakoyun, N., Kubilay, S., Aktas, N., Turhan, O., Kasimoglu, M., Yilmaz, S., & Sahiner, N. (2011). Hydrogel–biochar composites for effective organic contaminant removal from aqueous media. *Desalination, 280*(1–3), 319–325.

Kholssi, R., Marks, E. A., Montero, O., Mat´e, A. P., Debdoubi, A., & Rad, C. (2018). The growth of filamentous microalgae is increased on biochar solid supports. *Biocatalysis and Agricultural Biotechnology, 13*, 182–185.

LeBel, C. P., Ischiropoulos, H., & Bondy, S. C. (1992). Evaluation of the probe 2′, 7′-dichlorofluorescin as an indicator of reactive oxygen species formation and oxidative stress. *Chemical Research in Toxicology, 5*(2), 227–231.

Lee, J., Park, S., Roh, H.-G., Oh, S., Kim, S., Kim, M., … Park, J. (2018). Preparation and characterization of superabsorbent polymers based on starch aldehydes and carboxymethyl cellulose. *Polymers, 10*(6), 605.

Liu, P., Xu, H., Mi, X., Xu, L., & Yang, Y. (2015). Oxidized sucrose: A potent and biocompatible crosslinker for three-dimensional fibrous protein scaffolds. *Macromolecular Materials and Engineering, 300*(4), 414–422.

Liu, Y., Wang, J., Chen, H., & Cheng, D. (2022). Environmentally friendly hydrogel: A review of classification, preparation and application in agriculture. *Science of the Total Environment, 846*, Article 157303.

Mashkour, M., Rahimnejad, M., & Mashkour, M. (2016). Bacterial cellulose-polyaniline nano-biocomposite: A porous media hydrogel bioanode enhancing the performance of microbial fuel cell. *Journal of Power Sources, 325*, 322–328.

Mathiot, C., Ponge, P., Gallard, B., Sassi, J.-F., Delrue, F., & Le Moigne, N. (2019). Microalgae starch-based bioplastics: Screening of ten strains and plasticization of unfractionated microalgae by extrusion. *Carbohydrate Polymers, 208*, 142–151.

Peng, D., Ouyang, F., Deng, M., Nie, L., & Kong, S. (2021). A comprehensive characterization of different fractions of corn stover and their relationships to multipollutant sorption characteristics. *Adsorption Science & Technology, 2021*, 1–19.

Qureshi, M. A., Nishat, N., Jadoun, S., & Ansari, M. Z. (2020). Polysaccharide based superabsorbent hydrogels and their methods of synthesis: A review. *Carbohydrate Polymer Technologies and Applications, 1*, Article 100014.

Rahman, Q. M., Zhang, B., Wang, L., & Shahbazi, A. (2019). A combined pretreatment, fermentation and ethanol-assisted liquefaction process for production of biofuel from Chlorella sp. *Fuel, 257*, Article 116026.

Reddy, N., & Yang, Y. (2010). Citric acid cross-linking of starch films. *Food Chemistry, 118*(3), 702–711.

Rimdusit, S., Somsaeng, K., Kewsuwan, P., Jubsilp, C., & Tiptipakorn, S. (2012). Comparison of gamma radiation crosslinking and chemical crosslinking on properties of methylcellulose hydrogel. *Engineering Journal, 16*(4), 15–28.

Rioux, B., Ispas-Szabo, P., Aı¨t-Kadi, A., Mateescu, M.-A., & Juhasz, J. (2002).´ Structure–properties relationship in cross-linked high amylose starch cast films. *Carbohydrate Polymers, 50*(4), 371–378.

Rosli, S. S., Kadir, W. N. A., Wong, C. Y., Han, F. Y., Lim, J. W., Lam, M. K., … Usman, A. (2020). Insight review of attached microalgae growth focusing on support material packed in photobioreactor for sustainable biodiesel production and wastewater bioremediation. *Renewable and Sustainable Energy Reviews, 134*, Article 110306.

Sajjadi, B., Chen, W.-Y., Raman, A. A. A., & Ibrahim, S. (2018). Microalgae lipid and biomass for biofuel production: A comprehensive review on lipid enhancement strategies and their effects on fatty acid composition. *Renewable and Sustainable Energy Reviews, 97*, 200–232.

Sakhiya, A. K., Anand, A., & Kaushal, P. (2020). Production, activation, and applications of biochar in recent times. *Biochar, 2*(3), 253–285.

Salehi, B., & Wang, L. (2022). Critical review on nanomaterials for enhancing bioconversion and bioremediation of agricultural wastes and wastewater. *Energies, 15*(15), 5387.

Shahbazi, M., Ahmadi, S. J., Seif, A., & Rajabzadeh, G. (2016). Carboxymethyl cellulose film modification through surface photo-crosslinking and chemical crosslinking for food packaging applications. *Food Hydrocolloids, 61*, 378–389.

Singh, B., Dolk, M. M., Shen, Q., & Camps-Arbestain, M. (2017). Biochar pH, electrical conductivity and liming potential. In *Biochar: A guide to analytical methods* (p. 23).

Thomas, D., Fernandez, N. B., Mullassery, M. D., & Surya, R. (2020). Iron oxide loaded biochar/polyaniline nanocomposite: Synthesis, characterization and electrochemical analysis. *Inorganic Chemistry Communications, 119*, Article 108097.

Torkamani, S., Wani, S., Tang, Y., & Sureshkumar, R. (2010). Plasmon-enhanced microalgal growth in miniphotobioreactors. *Applied Physics Letters, 97*(4).

Vargas-Estrada, L., Torres-Arellano, S., Longoria, A., Arias, D. M., Okoye, P. U., & Sebastian, P. (2020). Role of nanoparticles on microalgal cultivation: A review. *Fuel, 280*, Article 118598.

White, S. A., Strosnider, W. H., Chase, M. E., & Schlautman, M. A. (2021). Removal and reuse of phosphorus from plant nursery irrigation return water with reclaimed iron oxides. *Ecological Engineering, 160*, Article 106153.

Xu, H., Canisag, H., Mu, B., & Yang, Y. (2015). Robust and flexible films from 100% starch cross-linked by biobased disaccharide derivative. *ACS Sustainable Chemistry & Engineering, 3*(11), 2631–2639.

Yamashita, T., & Hayes, P. (2008). Analysis of XPS spectra of Fe^{2+} and Fe^{3+} ions in oxide materials. *Applied Surface Science, 254*(8), 2441–2449.

Yang, L., He, L., Xue, J., Wu, L., Ma, Y., Li, H., … Zhang, Z. (2019). Highly efficient nickel (II) removal by sewage sludge biochar supported α-Fe2O3 and α-FeOOH: Sorption characteristics and mechanisms. *PLoS One, 14*(6), Article e0218114.

Zhang, B., Wang, L., Li, R., Rahman, Q. M., & Shahbazi, A. (2017). Catalytic conversion of chlamydomonas to hydrocarbons via the ethanol-assisted liquefaction and hydrotreating processes. *Energy & Fuels, 31*(11), 12223–12231.